

SID



بلاگ مرکز اطلاعات علمی



کارگاه‌های آموزشی



سرویس ترجمه تخصصی



فیلم‌های آموزشی

کارگاه‌ها و فیلم‌های آموزشی مرکز اطلاعات علمی

آشنایی با پایگاه‌های اطلاعات علمی بین‌المللی و ترندهای جستجو بین‌المللی و ترندهای جستجو

کاربرد نرم افزار SPSS در پژوهش

بروبوزال نویسی (علوم انسانی)

کاربرد نرم‌افزار End Note در استناددهی مقالات و متون علمی

صدور گواهینامه نمایه مقالات نویسندگان در SID

FULL PAPER

Synthesis and characterization of silver nanoparticles-doped mesoporous bioactive glass prepared by spray pyrolysis

Tayseer A. Kareem* | Dunia K. Mahdi

Department of Physics, College of Science, University of Baghdad, Baghdad, Iraq

In the present work, we establish that Ag-doped mesoporous bioactive glass (MBG) can be prepared by spray pyrolysis (SP) process. This process offers the feature of low processing times and continuous production. This work was prepared in two steps, the first step was to prepare the material (MBG), and the second step was to make a nano-layer of silver material on the surface of the (MBG) according to the time interval between two spray processes (2, 4, and 6 min). Using scanning electron microscopy (SEM), energy dispersive X-Ray analysis (EDX), UV-Vis spectroscopy, and Fourier transform infrared spectroscopy (FTIR) were used to analyze the sample. According to the SEM and EDX Analysis result, the suitable formulation of the precursors can be used to control the distribution of the Ag dopant nanoparticles within MBGs. Also, UV-Vis shows that the absorption coefficient as a function of $h\nu$ (eV) and the extinction coefficient as a function of λ take the same behavior.

***Corresponding Author:**

Tayseer A. Kareem

Email: tayseer.kareem1204@sc.uobaghdad.edu.iq

Tel.: + 964 780 426 7203

KEYWORDS

Bioactive glass; spray pyrolysis; porous; MBGs.

Introduction

Bioactive glasses (BGs) are attractive materials for tissue regeneration because of their biocompatibility, angiogenic and osteogenic characteristics [1]. Nanoscale BGs, are particularly attractive material in biomedical applications. For example, it can be used in coating [2], scaffolds [3], and hydrogels [4] as advanced bioactive filler to improve the matrices functionalities (e.g. mechanical properties, biomineralization ability, and osteogenesis), because of their morphological benefits (e.g., low dimension, uniform size, controllable shape) [5]. Mesoporous bioactive glass nanoparticles (MBGN), among many nanoscale BGs, are gaining popularity in tissue regeneration, or nanomedical application as bioactive fillers or

drug carriers due to their large surface to volume ratio, wide specific surface area, and customizable size/pore structure [2]. The application field of MBGs has moved a big step forward by including a controllable amount of different ions in their composition [6]. The chemical composition of BGs, in addition to their morphology, can be modified for specific uses [7]. Silver (Ag), for example, can be added to BGs to boost their antibacterial activity [8]. Infections caused by bacteria continue to be a significant clinical obstacle for repairing and regenerating efficient tissue [9-11]. Alternatively, using antibacterial materials may reduce the infection risk without the bacterial resistance problem [10-12]. There is a high need for antibacterial formulations employed in tissue regeneration therapies.

Antibacterial metal ions have been around for a long time [13], and Ag has been shown to have good broad-spectrum bactericidal activity [14]. Adding Ag to BGs may enhance their antibacterial properties [15]. It is possible to produce mesoporous bioactive glass nanoparticles (MBGN) containing silver metal in two ways: one-step and post-modification. Firstly, Ag precursors (typically soluble silver salts) are introduced to create and for BGN [16, 17]. In the second method, Different metal ions (such Ca and Ag) have been inserted after BGN formation while

maintaining the produced nanoparticles' form, size, and porosity [17].

In this research, Ag-doped MBGs were synthesized using the spray pyrolysis method with different deposition time at 400 C and studied the optical and structural properties

Materials and methods

Synthesis of Ag-MBG Nanoparticles

The preparation of Ag-MBG nanoparticles by chemical spray pyrolysis method was illustrated in Figure 1.

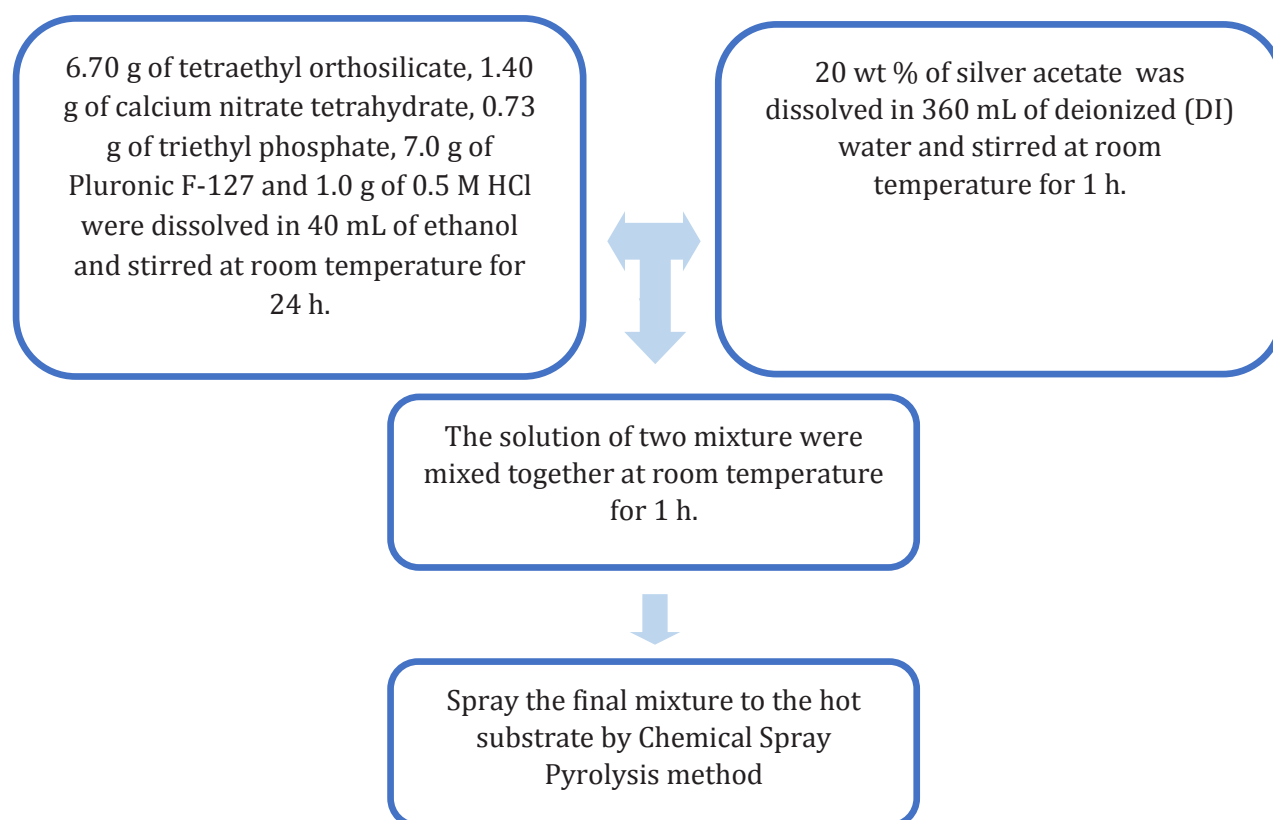


FIGURE 1 Flow chart of prepared Ag-doped MBG nanoparticles

Formation of Ag-MBG nanoparticle sample

The Ag-doped MBG nanoparticle is formed on a hot glass sheet substrate by the chemical spray pyrolysis system shown in Figure 2. The glass sheets were distributed on the hot plate, and the preparing solution was sprayed when the temperature of the heater reached 400 °C.

The spraying operation continued fifteen times with 2 s spraying time, and the time interval between two spray processes was equal to 2, 4, and 6 min. Then, the layer appeared on the surface of the substrate, and nanostructure Ag-doped MBG particles were formed.

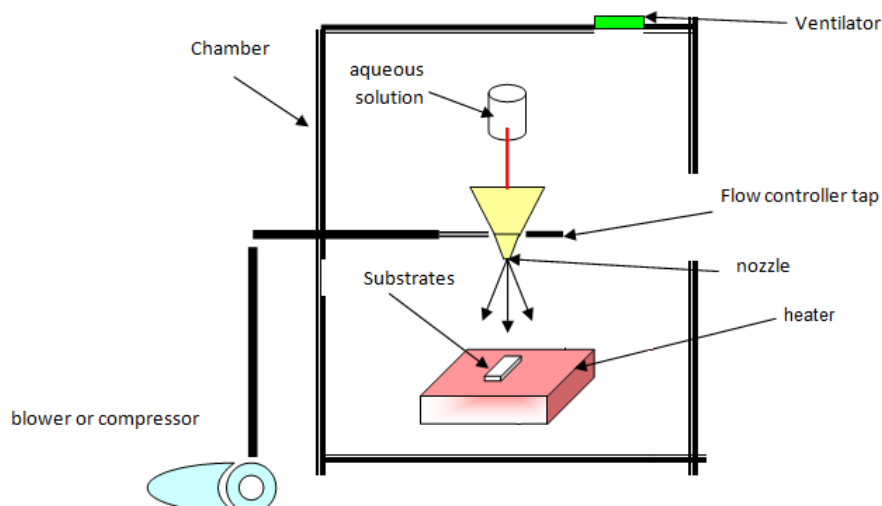


FIGURE 2 Spray pyrolysis system

Characterization

The Absorption measurement was tested using UV-VIS spectrophotometer type (Lambda 365, USA).

Field emission scanning electron microscopy (FE-SEM, model TESCAN MIRA3, French) with a 10-mm squared active area was used to assess the surface morphology of produced powders.

Fourier transform infrared spectrophotometer (FTIR, model Perkin Elmer Frontier) was used to obtain the infrared spectra of the produced glasses. The spectra were recorded using Fourier transform spectrometer near, mid, and far-infrared ranges.

Results and discussion

Temperature is one of the critical parameters in preparing nanoparticles. It has a significant effect on the homogeneity of the prepared nanoparticle because it is responsible for the varying crystal structure of the material. The temperature of 400 C shows the best results because the particles return to aggregate by increasing it. The structure and composition of

Ag-MBG were evaluated using the SEM and EDX analysis, as shown in Figure 3. Figure 3 reveals Ag-MBG particles' surface at 400 °C with a different time interval between two spray processes (2, 4, and 6 min).

At 2 min of spray deposition, SEM shows that their surfaces were heterogeneous agglomerates (nanoparticles) with different sizes (16-22 nm) were observed in the structure, which is an expected case since the spray precipitation technique relies on the nucleation-aggregation-agglomeration-growth mechanism. Their EDX spectra show a significant amount of Si and a small amount of O, Ca, C and Ag.

As for the time of 4 min, SEM showed aggregation of spherical particles on sample surfaces with the increase in the size of the nanoparticles (13-24 nm). Their EDX spectrum of the new surface layer showed higher concentrations of Si with a slight increase of O, Ca, C and Ag.

At 6 min, the surface was almost homogeneous, covered by a layer of Ag-nanoparticles that diameters range from (24 to 33 nm), with a slight increase of O, Ca, C, and Ag.

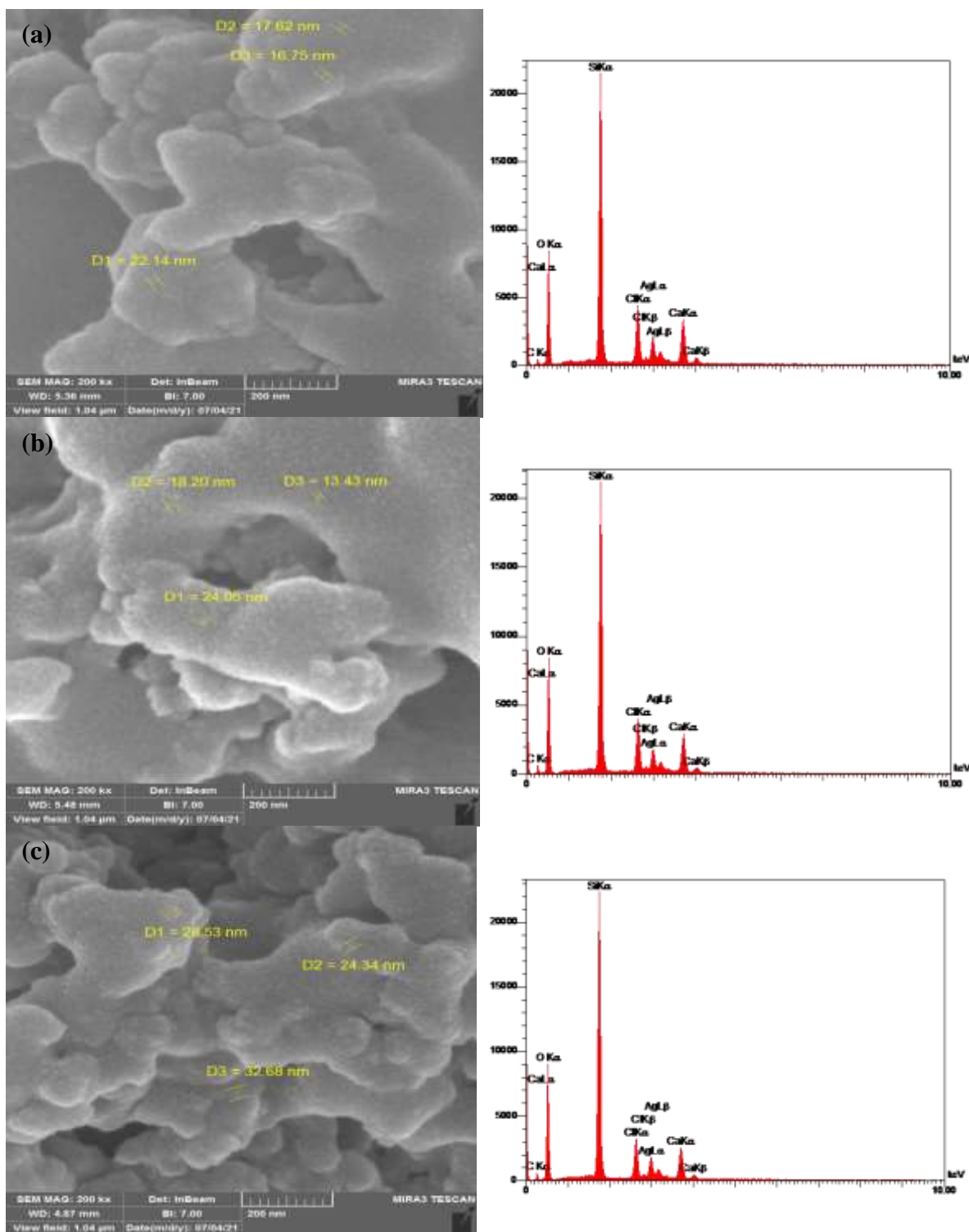
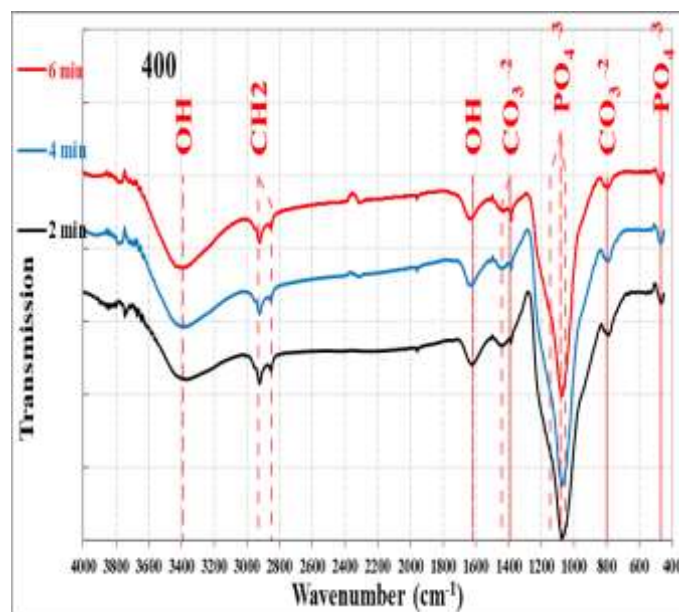


FIGURE 3 SEM micrographs of Ag-MBG sample followed by EDX analysis with time interval between two spray processes (a (2 min), b (4 min), and c (6 min)) at 400 C

The FTIR spectrum observed the chemical structure and the bond between MBG and Ag nanoparticles. Figure 4 demonstrates the FTIR spectrum for the sample Ag-MBG with a time

interval between two spray processes (2, 4, and 6 min) respectively at 400 °C. The band type extracted from these spectrums was listed in the table behind it.



Band type	2 min	4 min	6 min
OH	3377.66	3384.04	3393.62
CH ₂	2921.28	2921.28	2924.47
	2854.26	2854.26	2854.26
OH	1622.34	1631.91	1635.11
CO ₃	1440.43	1443.62	1437.23
	1382.98	1382.98	1382.98
PO ₄	1073.40	1070.21	1070.21
CO ₃	789.36	795.75	795.75
PO ₄	467.02	467.02	460.64

FIGURE 4 FTIR spectra of the samples Ag-MBG with the time interval between two spray processes of 2, 4, and 6 min at 400 C

The optical properties were examined by measuring the transmittance of the film in the visible region of the electromagnetic spectrum Ag-MBG thin film is not very transparent. The

maximum transmittance is about (2%, 15%, 53%) recorded for the time of spray pyrolysis 2, 4, and 6 min, as shown in Figure 5.

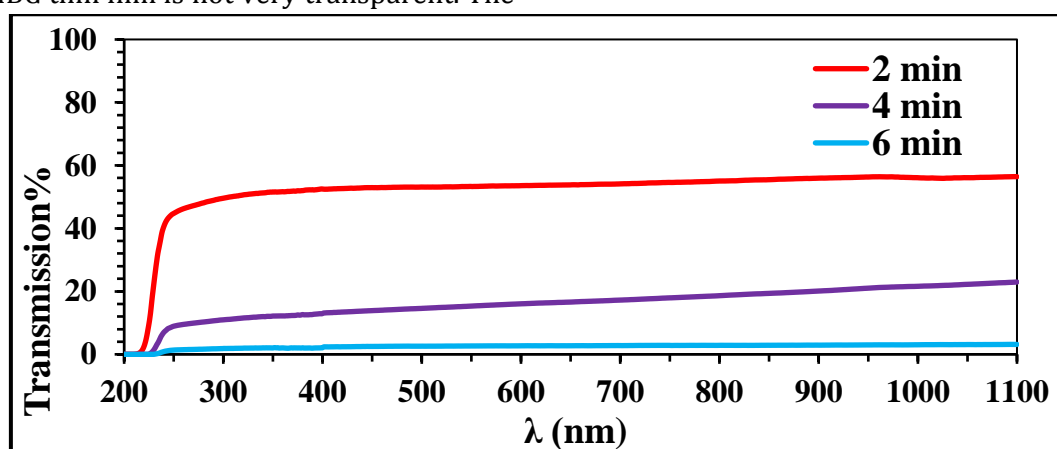


FIGURE 5 The transmittance spectrum of the samples Ag-MBG with the time interval between two spray processes of 2, 4, and 6 min at 400 C

The surface plasmon resonance of the samples was reported in the wavelength range of 200-1000 nm using a UV-VIS spectrophotometer in addition to the substance structure and chemical

characterization. As the time interval increased (2, 4, and 6 min), the absorption increased due to the thickness increasing (Figure 6).

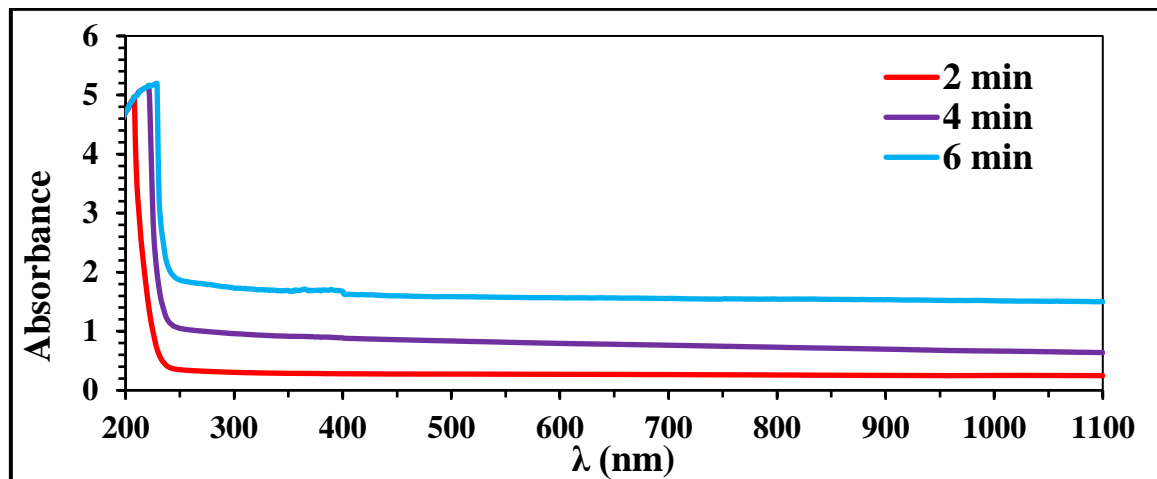


FIGURE 6 The Absorbance spectrum of the samples Ag-MBG with the time interval between two spray processes (2, 4, and 6 min) at 400 C

Figure 7 shows the absorption coefficient (α) variation with wavelength variation for Ag-MBG thin film. The relation shows that the

absorption coefficient increases with increasing the time interval from (2, 4, and 6 min) min, respectively.

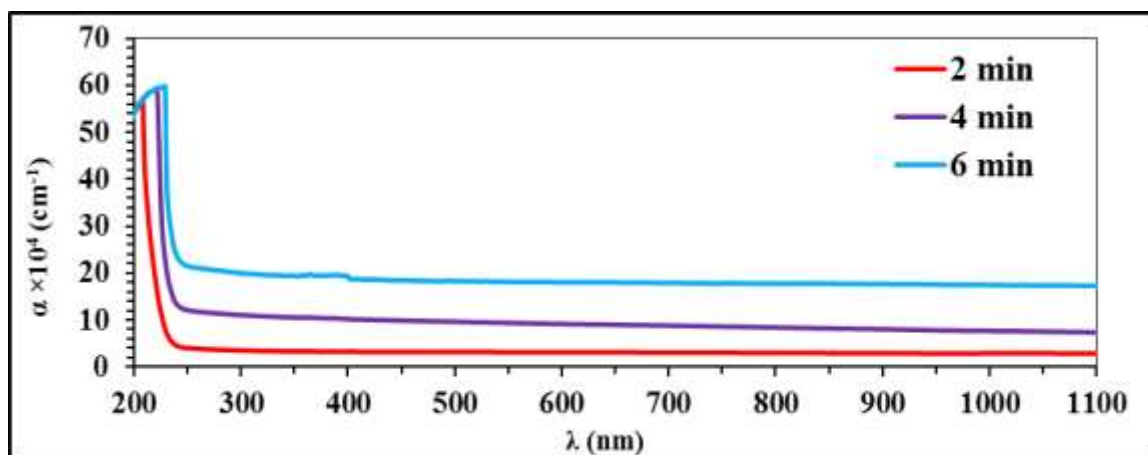


FIGURE 7 The relation between absorption coefficient and the wavelength of the samples Ag-MBG with the time interval between two spray processes (2, 4, and 6 min) at 400 C

From these results, one can calculate the energy band gap. Figure (8) shows that the absorption coefficient (α) for examined thin film increases as photon energy increases. The absorption coefficient has values (which

increases the possibility of a direct transition occurring). Also, the extinction coefficient as a function of λ exhibits the same behavior of α as a function of $h\nu$ (eV). Figure (8) shows the direct energy gap for Ag-MBG thin films.

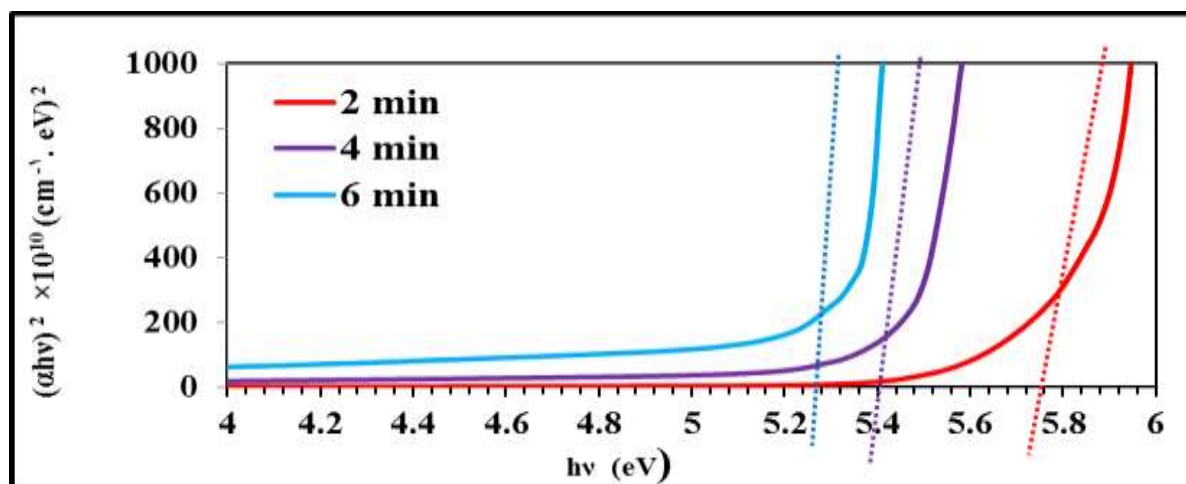


FIGURE 8 The relation between absorption coefficient and the wavelength of the samples Ag-MBG with the time interval between two spray processes (2, 4, and 6 min) at 400 C

The Urbach energy, which values are reported in Table 1, provides information about the localized state in the band gap. This effect can be explained by rising packing

density as the degree of amorphousness of the films decreases, resulting in decreasing in localized state.

TABLE 1 Optical parameters for Ag-MBG thin film

Time (min)	T%	α (cm ⁻¹)	K	N	ϵ_r	ϵ_i	E _g (eV)
2	53.32	31447	0.138	4.425	19.560	1.219	5.80
4	15.33	93784	0.411	9.099	82.621	7.473	5.48
6	2.66	181334	0.794	7.382	53.858	11.723	5.36

Conclusion

The SEM images of the Ag-doped MBG particles revealed that the particles were spherical at all periods investigated. At 6 min. The surface was almost homogeneous, covered by a layer of Ag-nanoparticles with diameters ranging from (24 to 33 nm). The variation of the absorption coefficient (α) with wavelength variation for Ag-MBG thin film shows that the absorption coefficient increases with increasing the time interval (2, 4, and 6 min), respectively. In addition, the absorption coefficient as a function of $h\nu$ (eV) and the extinction coefficient as a function of λ take the same behavior.

Acknowledgements

Institute of laser for postgraduate studies, University of Baghdad, supported this work.

References

- [1] J.R. Jones, *Acta Biomater.*, **2015**, *23*, S53–S82. [[Crossref](#)], [[Google Scholar](#)], [[Publisher](#)]
- [2] K. Zheng, A.R. Boccaccini, *Adv. Colloid Interf. Sci.*, **2017**, *249*, 363–373. [[Crossref](#)], [[Google Scholar](#)], [[Publisher](#)]
- [3] Y. Yang, K. Zheng, R. Liang, A. Mainka, N. Taccardi, J.A. Roether, R. Detsch, W.H. Goldmann, S. Virtanen, A.R. Boccaccini, *Biomed. Mater.*, **2018**, *13*, 015001. [[Crossref](#)], [[Google Scholar](#)], [[Publisher](#)]
- [4] K. Zheng, J. Wu, W. Li, D. Dippold, Y. Wan, A.R. Boccaccini, *ACS Biomater Sci. Eng.*, **2018**, *4*, 1546–1557. [[Crossref](#)], [[Google Scholar](#)], [[Publisher](#)]
- [5] C.D.F. Moreira, S.M. Carvalho, H.S. Mansur, M.M. Pereira, *Mater. Sci. Eng. C*, **2016**, *58*, 1207–1216. [[Crossref](#)], [[Google Scholar](#)], [[Publisher](#)]

- [6] A. Bari, N. Bloise, S. Fiorilli, G. Novajra, M. Vallet-Regí, G. Bruni, A. Torres-Pardo, J.M. González-Calbet, L. Visai, C. Vitale-Brovarone, *Acta Biomaterialia*, **2017**, *55*, 493-504. [[Crossref](#)], [[Google Scholar](#)], [[Publisher](#)]
- [7] S. Kaya, M. Cresswell, A.R. Boccaccini, *Mater. Sci. Eng. C.*, **2017**, *83*, 99-107. [[Crossref](#)], [[Google Scholar](#)], [[Publisher](#)]
- [8] J.H. Lee, A. El-Fiqi, N. Mandakbayar, H.H. Lee, H.W. Kim, *Biomaterials*, **2017**, *142*, 62-76. [[Crossref](#)], [[Google Scholar](#)], [[Publisher](#)]
- [9] W. Fan, Y. Wu, T. Ma, Y. Li, B. Fan, *J. Mater. Sci. Mater. Med.*, **2016**, *27*, 16-25. [[Crossref](#)], [[Google Scholar](#)], [[Publisher](#)]
- [10] C.R. Arciola, D. Campoccia, L. Montanaro, *Nat. Rev. Microbiol.*, **2018**, *16*, 397-409. [[Crossref](#)], [[Google Scholar](#)], [[Publisher](#)]
- [11] I. Denry, L.T. Kuhn, *Dent. Mater.*, **2016**, *32*, 43-53. [[Crossref](#)], [[Google Scholar](#)], [[Publisher](#)]
- [12] M. Shi, Z. Chen, S. Farnaghi, T. Friis, X. Mao, Y. Xiao, C. Wu, *Acta Biomater.*, **2016**, *30*, 334-344. [[Crossref](#)], [[Google Scholar](#)], [[Publisher](#)]
- [13] F.E. Ciraldo, E. Boccardi, V. Melli, F. Westhauser, A.R. Boccaccini, *Acta Biomater.*, **2018**, *75*, 3-10. [[Crossref](#)], [[Google Scholar](#)], [[Publisher](#)]
- [14] S. Chernousova, M. Epple, *Chem. Int. Ed.*, **2013**, *52*, 1636-1653. [[Crossref](#)], [[Google Scholar](#)], [[Publisher](#)]
- [15] H.N. Wilkinson, S. Iveson, P. Catherall, M.J. Hardman, *Front. Microbiol.*, **2018**, *9*, 1450-1466. [[Crossref](#)], [[Google Scholar](#)], [[Publisher](#)]
- [16] K. Gold, B. Slay, M. Knackstedt, A.K. Gaharwar, *Adv. Ther. One*, **2018**, 1700033. [[Crossref](#)], [[Google Scholar](#)], [[Publisher](#)]
- [17] D. Kozon, K. Zheng, E. Boccardi, Y. Liu, L. Liverani, A.R. Boccaccini, *Materials (Basel)*, **2016**, *9*, 225-233. [[Crossref](#)], [[Google Scholar](#)], [[Publisher](#)]

How to cite this article: Tayseer A. Kareem*, Dunia K. Mahdi. Synthesis and characterization of silver nanoparticles-doped mesoporous bioactive glass prepared by spray pyrolysis. *Eurasian Chemical Communications*, 2022, 4(4), 330-337. **Link:** http://www.echemcom.com/article_145019.html

SID



بلاگ مرکز اطلاعات علمی



کارگاه‌های آموزشی



سرویس ترجمه تخصصی



فیلم‌های آموزشی

کارگاه‌ها و فیلم‌های آموزشی مرکز اطلاعات علمی

آشنایی با پایگاه‌های اطلاعات علمی بین‌المللی و ترندهای جستجو
بین‌المللی و ترندهای جستجو

کاربرد نرم افزار SPSS در پژوهش

بروبوزال نویسی (علوم انسانی)

کاربرد نرم‌افزار End Note در استناددهی مقالات و متون علمی

صدور گواهینامه نمایه مقالات نویسندگان در SID